Ceramics International 50 (2024) 34164–34172

Contents lists available at ScienceDirect

Ceramics International

journal homepage: www.elsevier.com/locate/ceramint

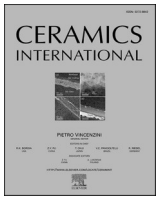

Synthesis of Si_3N_4 powder with a controllable alpha/beta ratio by sol-gel assisted carbothermal reduction and nitridation

Yan Wang, Zeyu Wang, Zeping Zhu, Jiaqi Wang, Ziyang Meng, Deqiang Wang *

School of Materials Science and Engineering, East China University of Science and Technology, Shanghai, 200237, China

ARTICLE INFO

Handling editor: P. Vincenzini

Keywords:
Si_3N_4
Phase transformation
Sol-gel processes
Whiskers

ABSTRACT

The controllable α/β ratio of Si_3N_4 powder was synthesized using tetraethyl orthosilicate (TEOS), glucose, $MgCl_2$ and $YCl_3{\cdot}6H_2O$ by sol-gel assisted carbothermal reduction and nitridation (CRN). This study aimed to investigate the impact of various parameters, including a H_2O/TEOS mol ratio of the sol, a C/Si mol ratio, sintering aids, and the temperature of CRN on the phase transformation of α-Si_3N_4. The results demonstrated that the H_2O/TEOS ratio significantly influenced the relative content of α and β phase in Si_3N_4 by changing the morphological characteristics of SiO_2. When the H_2O/TEOS ratio was 100, β-Si_3N_4 powder with an approximate β content over 88 wt% was synthesized at 1500 °C. This remarkable phase transformation was likely facilitated by the eutectic liquid phase consisting of $MgSiO_3$/Mg_2SiO_4. The SEM image revealed rod-like whiskers with a length around 1.4 μm for the β-Si_3N_4 grains. Due to the presence of liquid phase, the synthesis of spherical-like α-Si_3N_4 nano-powder with an α-phase content of 91 wt% was achieved at a lower temperature of 1450 °C, with an H_2O/TEOS ratio of 15 and a C/Si ratio of 4. The size of the particles was about 70 nm due to the reduced reaction temperature. Furthermore, without the addition of any sintering aids or Si_3N_4 seeds, high purity α-Si_3N_4 with an α phase content approaching 96 wt% could be synthesized at 1500 °C, using an H_2O/TEOS ratio of 15 and a C/Si ratio of 4. The resulting α-Si_3N_4 powder exhibited an extremely regular hexagonal prism shape with a length of approximately 2 μm.

1. Introduction

Si_3N_4 ceramic is expected to become the next-generation substrate for high-power devices due to its high thermal conductivity, strength, excellent thermal shock resistance, and low dielectric constant [1–6]. In order to achieve high-performance Si_3N_4 ceramic, it is crucial to prepare high-quality Si_3N_4 powder. The particle size, phase content, and particle morphology greatly influence the ceramic properties [7]. Consequently, the study of Si_3N_4 powder has always received significant attention from researchers. In general, there are two common crystalline forms of Si_3N_4: α-Si_3N_4 and β-Si_3N_4 [8]. While both belong to the hexagonal system, they differ in the length of the direction along the C-axis, which is caused by the stacking of atoms, resulting the difference of their property [9]. Additionally, under high-temperature and liquid phase conditions, α-Si_3N_4 spontaneously transforms to β-Si_3N_4 due to its unstable lattice structure [10]. Therefore, α-Si_3N_4 and β-Si_3N_4 have different preparation and application. The preparation of α-Si_3N_4 powder have various synthesis methods, such as nitridation of silicon, silicon-imide decomposition, and CRN [11–13]. High purity α-Si_3N_4 is usually used as the raw material of Si_3N_4 ceramic since it significantly improves the densification of ceramic during the sintering process [14]. The preparation of β-Si_3N_4 have been using α-Si_3N_4 as a raw material, Y_2O_3, MgO, or other oxides as sintering aids to promote the phase transformation from α-Si_3N_4 to β-Si_3N_4 at temperatures usually above 1700 °C [12,15]. This β-Si_3N_4 powder is typically applied as a filling material for high polymer materials to enhance their thermal conductivity [16,17]. Furthermore, by adjusting the α/β phase ratio of Si_3N_4, the advantages of both α-Si_3N_4 and β-Si_3N_4 can be combined, resulting in Si_3N_4 ceramic with unique properties achieved through changes in the microstructure [18]. For instance, Xing et al. [19] enhanced the mechanical properties of Si_3N_4 ceramic by in-situ growth of β-Si_3N_4 whiskers in Si_3N_4 powder. Yeh et al. [20] also found that substituting high-purity α or β-Si_3N_4 powder with (α+β)-Si_3N_4 significantly decreased the synthesis temperature of Sialon composite material. Therefore, α-Si_3N_4, β-Si_3N_4, and (α+β)-Si_3N_4 all have their own potential applications. However, to the best of our knowledge, there are few studies that focus on the preparation and influential factors of the phase transformation of Si_3N_4 powder. Moreover, there is a lack of a universal

* Corresponding author.
E-mail address: derek_wang@ecust.edu.cn (D. Wang).

https://doi.org/10.1016/j.ceramint.2024.06.234
Received 22 February 2024; Received in revised form 27 April 2024; Accepted 17 June 2024
Available online 18 June 2024

method capable of synthesizing not only the controllable α/β phase content of Si_3N_4 powder, but also high-purity α-Si_3N_4 and β-Si_3N_4 powder.

The CRN method offers significant advantages for potential industrial production of Si_3N_4 powder due to its cost-effectiveness and stability compared to other processes [21]. This technique utilizes SiO_2 and C as raw materials to synthesize Si_3N_4 powder under high temperatures and a flowing N_2 atmosphere, with the overall reaction equation outlined in Equation (1) [22,23].

$$3SiO_2(s)+6C(s)+2N_2(g) = Si_3N_4(s) +6CO(g) \quad (1)$$

However, a key limitation of the traditional CRN method lies in the extensive milling time required to achieve a uniform mixing state of the raw materials prior to high-temperature reaction [24]. This poses a challenge for efficient production. Sol-gel is a method commonly used to synthesize high-dispersity powder due to its ability to achieve homogeneous powder mixing and reduce the reaction temperature [25]. Therefore, combining the sol-gel and CRN methods offers a more efficient approach for Si_3N_4 powder production. Researchers in this field have made notable progress. For instance, Tan et al. [26] employed TEOS as silicon-source and glucose as carbon-source to synthesize precursor powder through sol-gel method. They postulated that the sol-gel approach significantly enhances the homogeneity of the raw materials compared to traditional mechanical mixing methods, thereby reducing the synthesis temperature required for Si_3N_4 powder. Their study demonstrated the synthesis of α-Si_3N_4 with a fibrous morphology at 1400 °C. Similarly, Zahra Omidi et al. [27] reported the synthesis of Si_3N_4 powder with spherical and fibrous morphologies using TEOS and saccharose as raw materials through the sol-gel method. They further investigated the impact of the C/Si ratio and reaction temperature on the growth of Si_3N_4 powder. Nonetheless, research on the synthesis of Si_3N_4 powder using TEOS and soluble carbon sources remains limited. And in the present research, both α-Si_3N_4 and β-Si_3N_4 coexist, but there is little research focusing on the phase transformation of the Si_3N_4 powder [26,28].

In this study, TEOS and glucose were used as the Si-source and C-source, respectively. $MgCl_2$ and $YCl_3{\cdot}6H_2O$ were used as sintering aids. The sol-gel and CRN processes were combined to synthesize Si_3N_4 powder with a controllable α/β ratio. The influence of the H_2O/TEOS mol ratio of the sol, the C/Si mol ratio, the temperature of CRN, and sintering aids on the phase transformation of Si_3N_4 were studied. Furthermore, the microstructure of Si_3N_4 powder and growth mechanism of β-Si_3N_4 were both investigated. Consequently, high-purity α-Si_3N_4 with different morphology and β-Si_3N_4 with whiskers structure were synthesized using the same process.

2. Material and methods

The starting materials of this study were all directly purchased from various companies. These materials include: TEOS (Shanghai Ling Feng Chemical Reagent Co., Ltd, Shanghai, China), $C_6H_{12}O_6{\cdot}H_2O$ (Shanghai Titan Technology Co., Ltd, Shanghai, China), $YCl_3{\cdot}6H_2O$ (Shanghai Titan Technology Co., Ltd, Shanghai, China), $MgCl_2$ (Shanghai Boer Chemical Reagents Co., Ltd, Shanghai, China), EtOH (Shanghai Boer Chemical Reagents Co., Ltd, Shanghai, China), HCl (Shanghai Ling Feng Chemical Reagent Co., Ltd, Shanghai, China), $NH_3{\cdot}H_2O$ (Shanghai Titan Technology Co., Ltd, Shanghai, China), deionized water. The starting materials were mixed according to Table 1. A lower water content was found to be unfavorable for dissolving glucose, therefore, the lowest R value was set to 15. After the mixing of the starting materials, HCl was added to bring a solution pH of 2. The solution was then placed in a water bath at 40 °C for 1 h to obtain a high dispersion transparent sol. Subsequently, $NH_3{\cdot}H_2O$ was added dropwise to the sol until the pH reached 8. The sol was aged for a 3 h to form a gel. The gel was crushed into pieces and dried in an oven at 80 °C for 8 h to obtain the precursor powder. The powder was then placed in a furnace, and the heating rate was set to 5 °C/min until it reached the final temperature. The CRN was performed at different reaction temperatures, including 1450 °C, 1500 °C, 1550 °C, and 1600 °C, for 4 h under high purity flowing nitrogen gas (purity 99.999 %) at a pressure of 0.1 Mpa. The gas flow rate was 300 mL/min. Finally, the powder was placed in a muffle furnace at 600 °C for 3 h to remove any excess carbon. The detailed schematic diagram of the process route was shown in Fig. 1.

Table 1
The starting composition of the raw materials and the label of the synthesized Si_3N_4 powder.

Number	R=H_2O/TEOS	C/Si	SSi/Y/Mgi	T/°C	Time/h	Label
1	15	3	93/2/5	1500	4	15-1500-4h-3C-YM
2	20					20-1500-4h-3C-YM
3	40					40-1500-4h-3C-YM
4	60					60-1500-4h-3C-YM
5	80					80-1500-4h-3C-YM
6	100					100-1500-4h-3C-YM
7	120					120-1500-4h-3C-YM
8	140					140-1500-4h-3C-YM
9	60	3	93/2/5	600	3	60-600-3h-3C-YM
10	80					80-600-3h-3C-YM
11	100					100-600-3h-3C-YM
12	120					120-600-3h-3C-YM
13	140					140-600-3h-3C-YM
14	100	3	93/2/5	1550	4	100-1550-4h-3C-YM
15				1600		100-1600-4h-3C-YM
16	15	3	93/2/5	1450	4	15-1450-4h-3C-YM
17		4				15-1450-4h-4C-YM
18		5				15-1450-4h-5C-YM
19	15	3	100/0/0	1450	4	15-1450-4h-3C
20		4				15-1450-4h-4C
21	15	3	100/0/0	1500	4	15-1500-4h-3C
22		4				15-1500-4h-4C

The obtained Si_3N_4 powder was analyzed for its phase composition using an X-ray diffractometer (XRD, Ultima IV, Rigaku Corporation, Japan) with Cu $K\alpha_1$ radiation. A step size of 0.02° (2θ) and a scanning rate of 8°/min were used. The (101) and (201) crystal planes of α-Si_3N_4 and the (101) and (200) crystal planes of β-Si_3N_4 were used to represent the different phase content of Si_3N_4. Equations (2) and (3) were used to calculate the β phase content and α phase content of Si_3N_4, respectively [29]. It was worth noting that this method assumed pure phase Si_3N_4 and the phase content was solely used for qualitative representation of the crystal phase ratio, not the actual content of each phase. Additionally, a field-emission scanning electron microscope (FESEM, GeminiSEM 500, Germany) equipped with an energy dispersive spectrometer (EDS) was used to investigate the microstructure, crystal size, and element composition of Si_3N_4. High-resolution transmission electron microscopy (HRTEM, JEM-2100, Japan) was used to observe the microstructure and lattice fringe of Si_3N_4. Dynamic Light Scattering (DLS, Zetasizer Nano series, Britain) was employed to determine the particle size distribution of Si_3N_4.

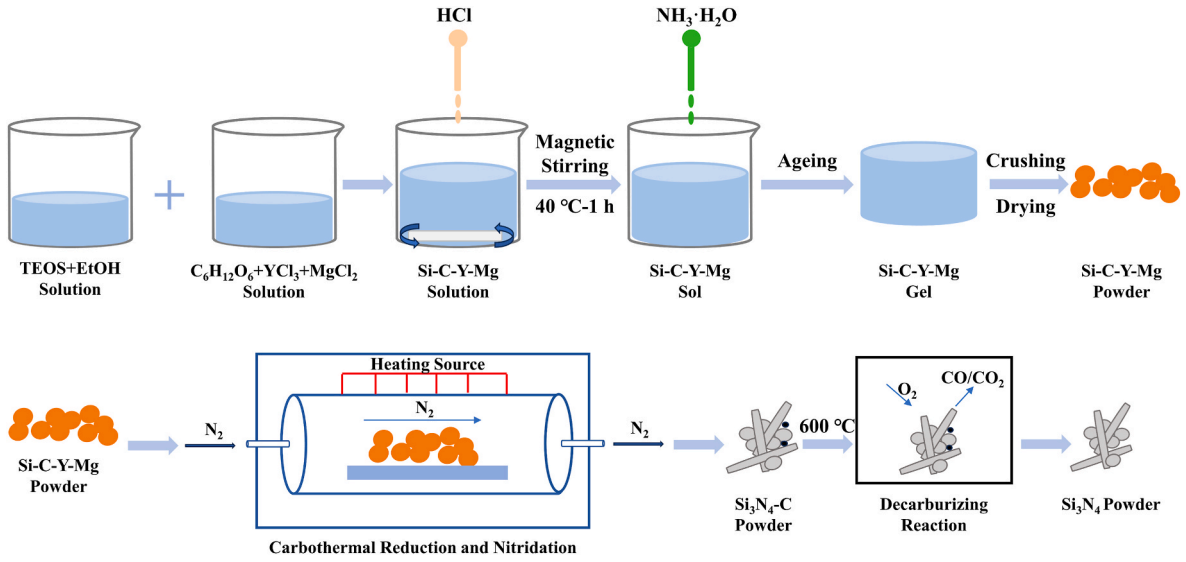

Fig. 1. The schematic diagram of preparation route for Si_3N_4 powder.

$$\beta(wt\%) = \frac{I_{\beta(101)} + I_{\beta(200)}}{I_{\beta(101)} + I_{\beta(200)} + I_{\alpha(101)} + I_{\alpha(201)}} \times 100\% \quad (2)$$

$$\alpha\ (wt\%) = 1\text{-}\beta\ (wt\%) \quad (3)$$

3. Results and discussion

3.1. Influence of the H_2O/TEOS ratio

The samples labeled R-1500-4h-3C-YM (R = 15 to 140) were used to investigate the influence of different H_2O/TEOS ratios (R) on the synthesis of Si_3N_4 powder, and the detailed parameters of the process were shown in Table 1. The XRD patterns of the Si_3N_4 powder could be seen from Fig. 2 (a). The main characteristic peaks were matched well with Si_3N_4, indicating the successful synthesis of Si_3N_4 powder. In addition, the corresponding crystalline phase of the peaks were marked as α and β, respectively, based on the position of the characteristic peaks of α-Si_3N_4 and β-Si_3N_4 (α-Si_3N_4, PDF#76–1407; β-Si_3N_4, PDF#76–1413). Interestingly, the relative peak intensities of α-Si_3N_4 and β-Si_3N_4 varied significantly with the increase in the R value. To demonstrate this change more clearly, the β phase content of Si_3N_4 was calculated using formula (2), and the detailed calculation process was provided in the supporting information. The results, shown in Fig. 2 (b), revealed that the β phase content of Si_3N_4 initially increased and then decreased with the continuous increase in the R value. Within the range of 15–100, the β phase content increased from a minimum of 14 wt% to almost 88 wt%. However, when the R value was in the range of 100–140, the β phase content began to decrease, from a maximum of 88 wt% to 32 wt%. These findings indicated that the α and β phase content of Si_3N_4 can be controlled to some extent by adjusting the H_2O/TEOS ratio of the sol.

To comprehensively investigate the factors contributing to the variation in β phase content in Si_3N_4 with different R values, a representative set of precursors spanning R values from 60 to 140 was selected for examining the morphological changes of SiO_2 produced by sol-gel process. Initially, these precursors were subjected to calcination at 600 °C for 3 h to eliminate H_2O and carbon, followed by characterization utilizing XRD and SEM techniques. The results were shown in Fig. 3 and 4. One of the XRD patterns of the precursors was depicted in Fig. 3, where a distinct broad peak at 2Theta = 23 indicated that the powder was amorphous SiO_2 after burning. The SEM images listed in Fig. 4 exhibited varying morphology of SiO_2 particles with different R values. It could be observed that as the R value increased, there was a significant change in the morphology of SiO_2 particles. Initially, it was evident that the primary particle size of the SiO_2 prepared via sol-gel process was extremely small, approximately around 40 nm, as illustrated by Fig. 4 (a), 4 (b) and 4 (c). Furthermore, the high surface energy of SiO_2 and gelation process resulted in the formation of a porous network structure, which facilitated the reduction reaction between

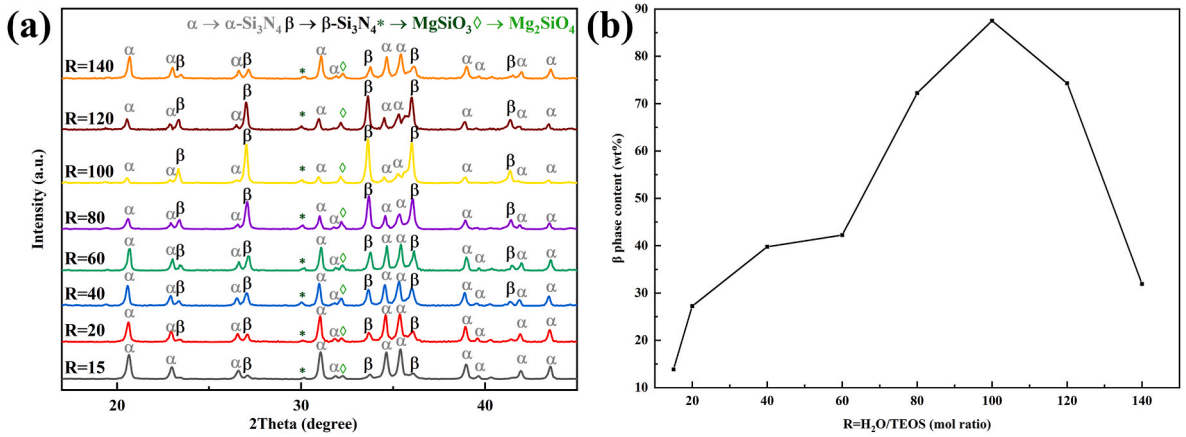

Fig. 2. The **(a)** XRD patterns and **(b)** line chart of β content variation with respect to R of Si_3N_4 powder synthesized at 1500 °C for 4 h with varying R values.

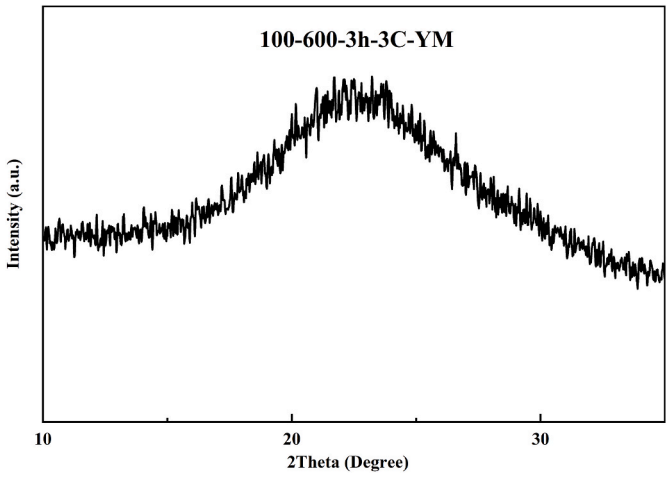

Fig. 3. XRD pattern of precursor with R = 100 at 600 °C for 3 h.

SiO_2 and C (Equation 4 (a) and 4 (b)) while promoting the N_2 flow. Consequently, this structure enhanced the synthesis rate of α-Si_3N_4 (Equation 5 (a) and 5 (b)) and then accelerated the phase transformation [30].

$$SiO_2(s) + C(s) = SiO(g) + CO(g) \quad 4(a)$$

$$SiO_2(s) + CO(g) = SiO(g) + CO_2(g) \quad 4(b)$$

$$3SiO(g)+3C(s)+2N_2(g) = Si_3N_4(s)+3CO(g) \quad 5(a)$$

$$3SiO(g)+3CO(g)+2N_2(g)=Si_3N_4(s)+3CO_2(g) \quad 5(b)$$

In addition, the obvious characteristic peaks corresponding to $MgSiO_3$ and Mg_2SiO_4 ($MgSiO_3$: PDF#35–0610; Mg_2SiO_4: PDF#72–0296) were observed in XRD patterns. It is known that $MgSiO_3$ and Mg_2SiO_4 are eutectic mixtures of SiO_2 and MgO [26,28]. Henceforth, it could be inferred that $MgCl_2$ used as sintering aid underwent subsequent reaction processes:

$$MgCl_2(s)+2NH_3{\cdot}H_2O(l) = Mg(OH)_2(s)+2NH_4Cl(s) \quad (6)$$

$$Mg(OH)_2(s) = MgO(s) + H_2O(g) \quad (7)$$

$$MgO(s) + SiO_2(s) = MgSiO_3(s) \quad (8)$$

$$2MgO(s) + SiO_2(s) = Mg_2SiO_4(s) \quad (9)$$

During the CRN process, $MgCl_2$ underwent a series of precipitation and dehydration reactions, ultimately leading to the formation of MgO, as outlined in Equations (6) and (7). Wang et al. [31] reported that the eutectic temperature of SiO_2 and MgO was about 1280 °C. Consequently, at a temperature of 1500 °C, a eutectic reaction occurred, as described by Equations (8) and (9). This phenomenon was further corroborated by the distinct characteristic peaks of $MgSiO_3$ and Mg_2SiO_4 observed in the XRD patterns, as shown in Fig. 2 (a). In the CRN process, the presence of a liquid phase not only accelerated mass transfer rate, but also dissolved α-Si_3N_4 particles and then promoted the phase transformation from α-Si_3N_4 to β-Si_3N_4 [32]. As a result, the low eutectic liquid phase formed by SiO_2 and MgO could accelerate solute transfer rate and wet the small particle α-Si_3N_4, which ultimately accelerated significant phase transformation of α-Si_3N_4 [33]. The mechanism for the formation of α-Si_3N_4 and the phase transformation from α-Si_3N_4 to β-Si_3N_4 with the process was shown in Fig. 5. Therefore, β-Si_3N_4 powder with β content reached nearly 88 wt% was synthesized at relatively low temperature (1500 °C). However, excessive H_2O content led to severe agglomeration of SiO_2 particles with block morphology observed in Fig. 4 (d). And the surface density increased with R = 140 from Fig. 4 (e). This was due to an excessive increase in water content that raised crosslinking degree and polymerization degree of gel leading to further agglomeration of SiO_2 [34]. Block-shaped SiO_2 had lower reactivity which was not conducive for gas-phase penetration. Therefore, the synthesis rate and transformation rate of α-Si_3N_4 were strongly decreased and resulting in significantly reduced β phase content in Si_3N_4.

In order to observe the microstructure of Si_3N_4 powder, samples with R values from 60 to 140 were selected for observation using SEM. As indicated in Fig. 6, distinct spherical-like and rod-like grains were observed. The EDS results of one of the Si_3N_4 powder were shown in Fig. 7, revealing that the rod-like grains (Fig. 7 (b)) and spherical-like grains (Fig. 7 (c)) consisted mainly of Si, N, with small amounts of C and O. The atomic percentage of Si and N was approximately 40 % and 51 % respectively, closely aligned with the theoretical composition of Si_3N_4, thus confirmed that both types of grains were indeed Si_3N_4. The rod-like whiskers were typical morphology of β-Si_3N_4, therefore, spherical-like grain should be α-Si_3N_4 [35,36]. The validity of this viewpoint can be corroborated by the lattice spacing measurements of Si_3N_4 obtained through HRTEM analysis [37]. As evident from Fig. 8 (b), the lattice spacing measured for rod-like Si_3N_4 was 0.380 nm, which aligns closely with the (110) lattice spacing characteristic of β-Si_3N_4. Similarly, Fig. 8 (d) revealed a lattice spacing of 0.259 nm for the

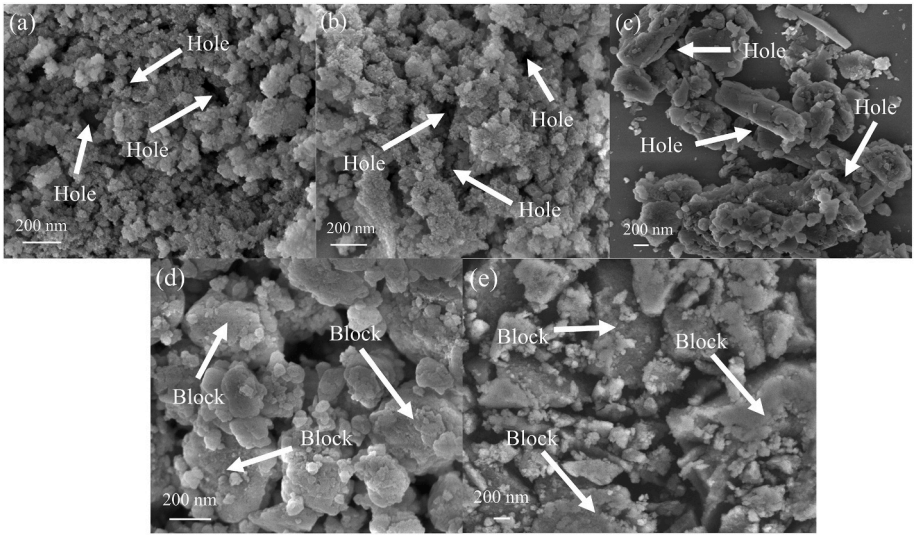

Fig. 4. The SEM images of SiO_2 from calcining of precursor with varying R values: **(a)** R = 60; **(b)** R = 80; **(c)** R = 100; **(d)** R = 120; **(e)** R = 140.

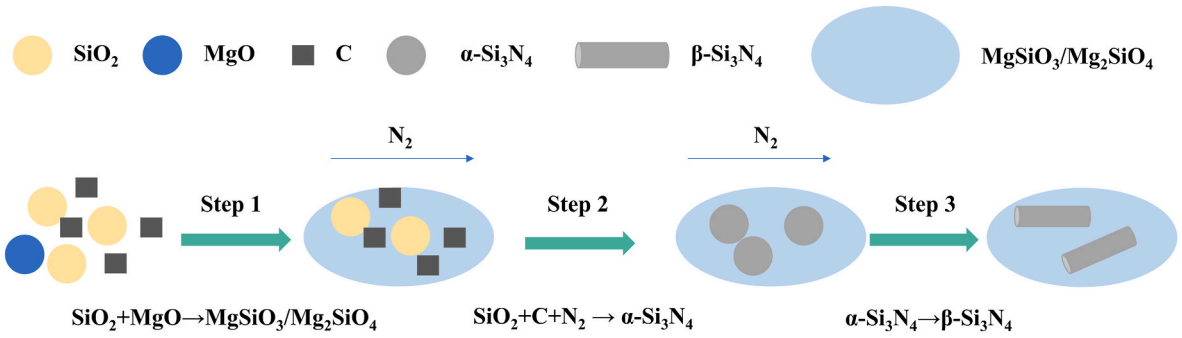

Fig. 5. The schematic diagram of phase transformation mechanism for Si_3N_4.

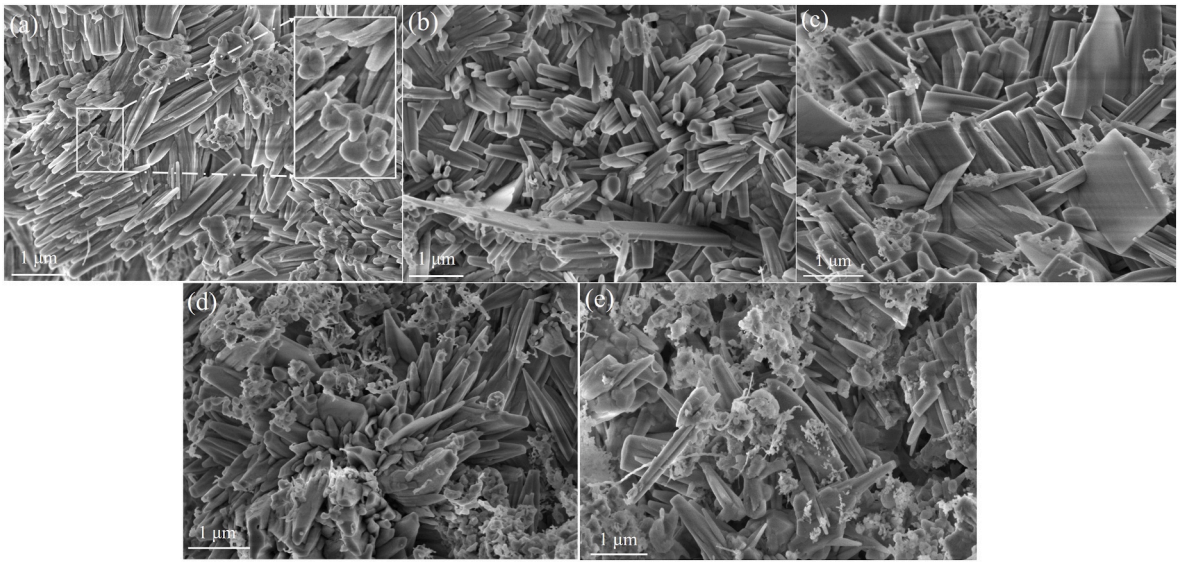

Fig. 6. The SEM images of Si_3N_4 powder synthesized with varying R values (**(a)** R = 60; **(b)** R = 80; **(c)** R = 100; **(d)** R = 120; **(e)** R = 140).

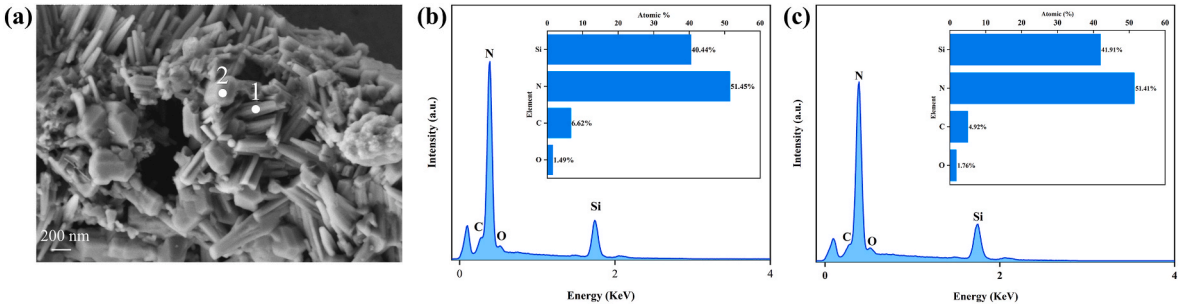

Fig. 7. SEM image **(a)** and EDS results (**(b)** the rod-like grain labeled as point 1; **(c)** the spherical-like grain labeled as point 2) of Si_3N_4 powder labeled 80-1500-4h-3C-YM.

spherical-like Si_3N_4, which corresponds well to the (102) lattice spacing of α-Si_3N_4. These observations provided strong support for the proposed viewpoint. Additionally, some irregularly shaped Si_3N_4 grains were observed at certain positions within the amplified section of Fig. 6 (a). These grains likely represented Si_3N_4 grains that were wet by liquid phase and have undergone incomplete phase transformation. Generally, the phase transformation of Si_3N_4 occurs via a dissolution-reprecipitation process. Initially, the α-Si_3N_4 grain dissolved in the liquid phase and then reprecipitated as β-Si_3N_4 through ion migration and grain growth [32]. Therefore, the irregularly shaped Si_3N_4 grains supported the presence of low eutectic liquid phase $MgSiO_3/Mg_2SiO_4$. Furthermore, as depicted in Fig. 6 (b) and 6 (c), the grain boundaries of Si_3N_4 became shaper with an increase in R value, indicating a gradual improvement in crystallinity with higher water content. Finally, Fig. 6 (d) and 6 (e) demonstrated a gradual increase in spherical-like Si_3N_4 grains, indicating a corresponding increase in α phase content with increasing R value.

The particle size distribution curve of Si_3N_4 powder with different R values was shown in Fig. 9. The curve exhibited three distinct peaks corresponding to particle sizes of 300 nm, 1 μm, and 5 μm, matched well with SEM results. The first peak at 300 nm represented spherical-like grains, predominantly composed of α-Si_3N_4 (Fig. 6 (a)). The second peak at 1 μm corresponded to rod-like grains, identified as β-Si_3N_4 (Fig. 6 (b)). The majority of particles fell within this size range. The last

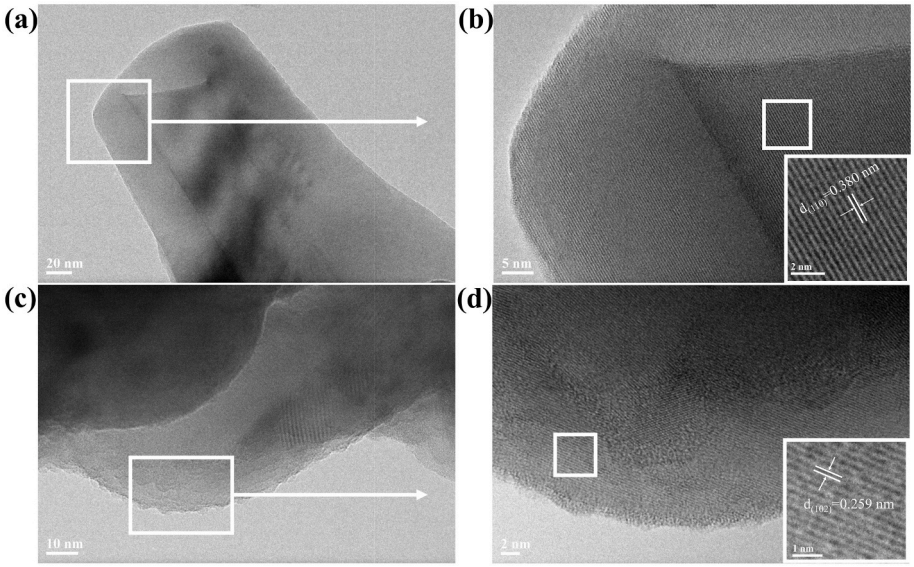

Fig. 8. TEM images of Si_3N_4 powder with rod-like whiskers (a, b) and spherical-like grain (c, d).

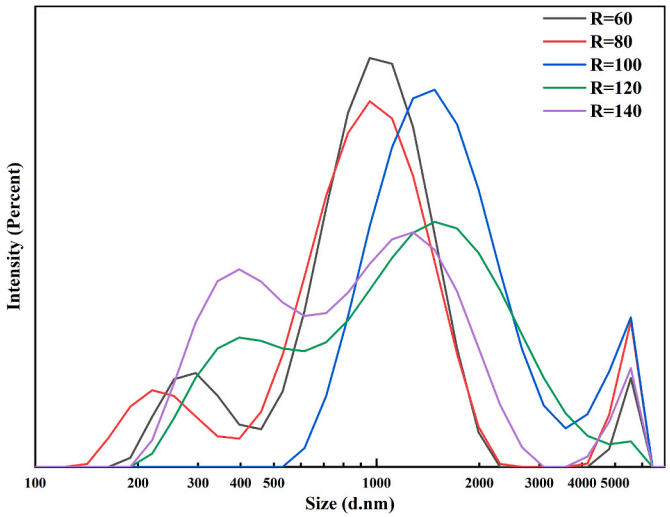

Fig. 9. The particle distribution curve of Si_3N_4 powder synthesized with varying R values.

peak corresponded to 5 μm and consisted of grains with abnormal shapes, such as the ribbon-like grain in Fig. 6 (b). In addition, the peak of the particle size distribution curve shifted to the right as the R value increased, indicating an enlargement in the grain size of Si_3N_4 with an increase in water content. This trend aligned with the observations from the SEM images. Furthermore, it was worth noting that the intensity of the peak corresponding to small α-Si_3N_4 particle sizes exhibited a noticeable trend. As the R value increased from 60 to 80, the intensity gradually decreased. At R = 100, the peak was almost absent. However, when the R value reached 120 and 140, the peak reappeared, and its intensity gradually magnified. This demonstrated a significant trend of initial decrease followed by subsequent increase, mirroring the variation in α phase content with R.

3.2. Influence of the reaction temperature

The reaction temperature of CRN is a crucial factor that significantly influences the phase transformation of Si_3N_4. In general, an increase in temperature leads to a decrease in the viscosity of liquid and promotes the phase transformation [38]. Therefore, Si_3N_4 powder labeled 100-1500-4h-3C-YM, 100-1550-4h-3C-YM, and 100-1600-4h-3C-YM were selected for investigating the impact of temperature of CRN, and the results were presented in Fig. 10. The line chart illustrating variations in β phase content of Si_3N_4 with temperature was shown in Fig. 10 (b). Contrary to expectations, as the temperature increased from 1500 °C to 1550 °C, there was a decrease in β phase content from 88 wt% to 56 wt%. And when temperature reached 1600 °C, there was a slight increase in β phase content to 59 wt%. These findings aligned with previous research by Alcala et al. [39], who observed a decrease in β phase content of Si_3N_4 from 22 wt% to 4 wt% after increasing the temperature by 135 °C. They attributed this phenomenon to difference in partial pressure of CO gas which could inhibit the phase transformation of α-Si_3N_4. Additionally, Fig. 10 (a) showed characteristic peaks corresponding to SiC (SiC, PDF#73–1708), which due to similar reaction temperatures between Si_3N_4 and SiC and greater stability of crystal structure exhibited by SiC compared to that of Si_3N_4. As a result, SiC was easily synthesized through Equation (10) when the temperature was high. Consequently, under high temperatures during this study, significant amounts of by-product SiC were synthesized simultaneously generating large quantities of CO gas which ultimately inhibited the phase transformation process within α-Si_3N_4. Therefore, the decrease observed in β phase content with increasing temperature may be due to the formation of by-product SiC at the relative low temperature.

$$SiO_2(s)+3C(s) = SiC(s)+2CO(g) \quad (10)$$

3.3. Influence of the C/Si

Weimer et al. [40] reported that α-Si_3N_4 has a tendency to synthesize in the presence of a large amount of carbon. Therefore, the influence of the C/Si molar ratio on the phase transformation of Si_3N_4 synthesized by sol-gel assisted CRN was investigated. The Si_3N_4 powder labeled 15-1450-4h-3C-YM, 15-1450-4h-4C-YM, and 15-1450-4h-5C-YM were studied using XRD and SEM. The XRD patterns were listed in Fig. 11 (a). It showed that all peaks of the synthesized Si_3N_4 match well with the standard peak, and the intensity of the α-Si_3N_4 peak was stronger than that of the β-Si_3N_4 peak, indicating the successful synthesis of α-Si_3N_4 with high α phase content. The α phase content of α-Si_3N_4 with different C/Si ratios was shown in Fig. 11 (b). The results revealed an increase from 88 wt% to 91 wt% as C/Si ratio increased from 3 to 4,

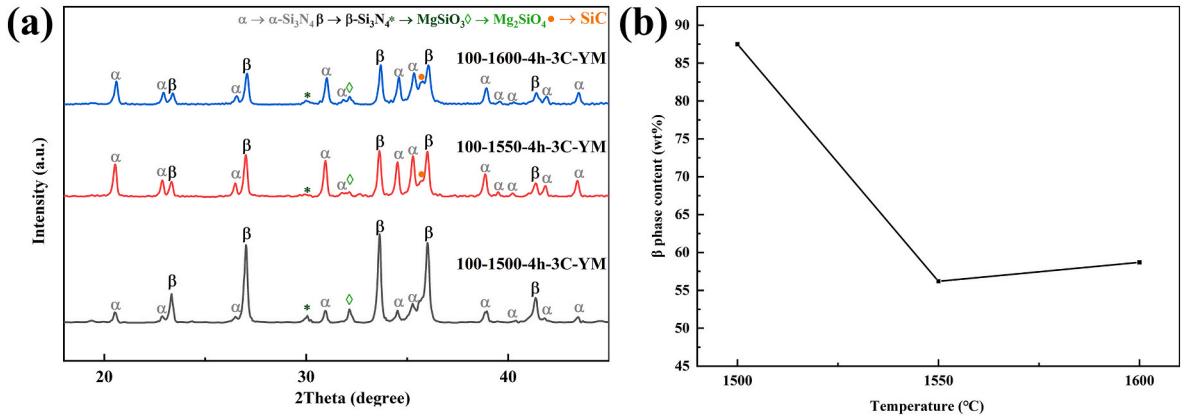

Fig. 10. The **(a)** XRD patterns and **(b)** line chart of β phase content variation with respect to temperature of Si_3N_4 powder synthesized at different reaction temperatures.

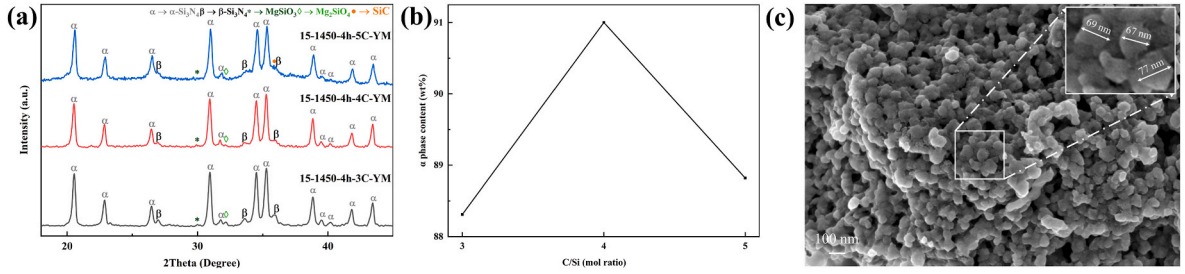

Fig. 11. The **(a)** XRD patterns of Si_3N_4 powder synthesized with different C/Si mol ratios; **(b)** line chart of α phase content variation with respect to C/Si mol ratio; **(c)** SEM image of Si_3N_4 powder labeled 15-1450-4h-4C-YM.

demonstrating that the carbon addition facilitated high purity α-Si_3N_4 powder synthesis. The SEM image of the α-Si_3N_4 could be observed in Fig. 11 (c), and it showed uniform spherical particles similar to those in Fig. 6 (a). In addition, due to the low temperature of CRN process, particle size was extremely small at approximately 70 nm, suggesting nano-spherical α-Si_3N_4 powder could be synthesized by reducing the temperature of CRN with adding sintering aids. However, excessive carbon led to formation of SiC as a by-product and decreased α phase content of Si_3N_4 (Equation (11)), according to the results of Si_3N_4 with C/Si ratio of 5 [32]. Therefore, a C/Si molar ratio of 4 was more suitable for synthesizing high purity α-Si_3N_4 powder.

$$Si_3N_4(s)+3C(s) = 3SiC(s)+2N_2(g) \quad (11)$$

3.4. Influence of sintering aids

The sample labeled 15-1450-4h-3C, 15-1450-4h-3C-YM, 15-1450-4h-4C, and 15-1450-4h-4C-YM were used for investigating the influence of sintering aids on the synthesis of Si_3N_4 powder. The XRD patterns of the samples were shown in Fig. 12 (a). It was evident that the intensity of all peaks of Si_3N_4 with added sintering aids (15-1450-3C-YM and 15-1450-4C-YM) was higher than that of Si_3N_4 without added sintering aids (15-1450-3C and 15-1450-4C). In particular, a distinct broad peak was observed in sample 15-1450-4C but not in sample 15-1450-4C-YM, indicating incomplete reaction without the addition of sintering aids. Additionally, peaks corresponding to $MgSiO_3$ and Mg_2SiO_4 were detected in the sample with sintering aids, demonstrating that the liquid phase formed by MgO and SiO_2 could accelerate solute transfer rate and promote the synthesis of Si_3N_4 powder [41]. Therefore, the addition of sintering aids was beneficial for synthesizing α-Si_3N_4 powder at low temperature.

However, it should be noted that the presence of a certain amount of liquid phase also promoted the phase transformation of Si_3N_4 which hindered achieving high purity α-Si_3N_4. To address this issue, gradual increase in temperature was employed instead of adding sintering aids. Therefore, Si_3N_4 powder labeled as 15-1500-4h-3C and 15-1500-4h-4C were synthesized for investigation, the XRD patterns were presented in Fig. 12 (b). Only characteristic peaks corresponding to Si_3N_4 were observed, indicating the successful synthesis of high purity Si_3N_4 powder. In fact, when the C/Si ratio was 4, the α phase content reached up to 96 wt%, illustrating the successful synthesis of high purity α-Si_3N_4 powder using this process. The SEM image of the high purity α-Si_3N_4 powder was shown in Fig. 12 (c) and 12 (d), which indicated that the cross profile of the grain was regular hexagon and the grain length was approximately about 2 μm. This demonstrated that the hexagonal prismatic α-Si_3N_4 crystal could be synthesized without adding sintering aids.

4. Conclusions

In this study, Si_3N_4 powder with controllable α and β phase content was synthesized using TEOS, glucose, $MgCl_2$, and $YCl_3{\cdot}6H_2O$ as raw materials by sol-gel assisted CRN process. The research also investigated various factors on the phase transformation of Si_3N_4, including the H_2O/TEOS ratio, the temperature of CRN, the C/Si ratio, and sintering aids. The experimental findings could be summarized as follows.

(1) The α and β phase contents of Si_3N_4 were significantly influenced by the H_2O/TEOS mol ratio in the sol. Increasing H_2O content greatly promoted the phase transformation of Si_3N_4 when the H_2O/TEOS ratio was below 100. However, excessive H_2O content restricted the phase transformation due to the severe agglomeration of SiO_2 caused by overhigh H_2O/TEOS ratio. The β-Si_3N_4 powder with β phase content reached nearly 88 wt% could be synthesized at 1500 °C for 4 h by using the H_2O/TEOS ratio of

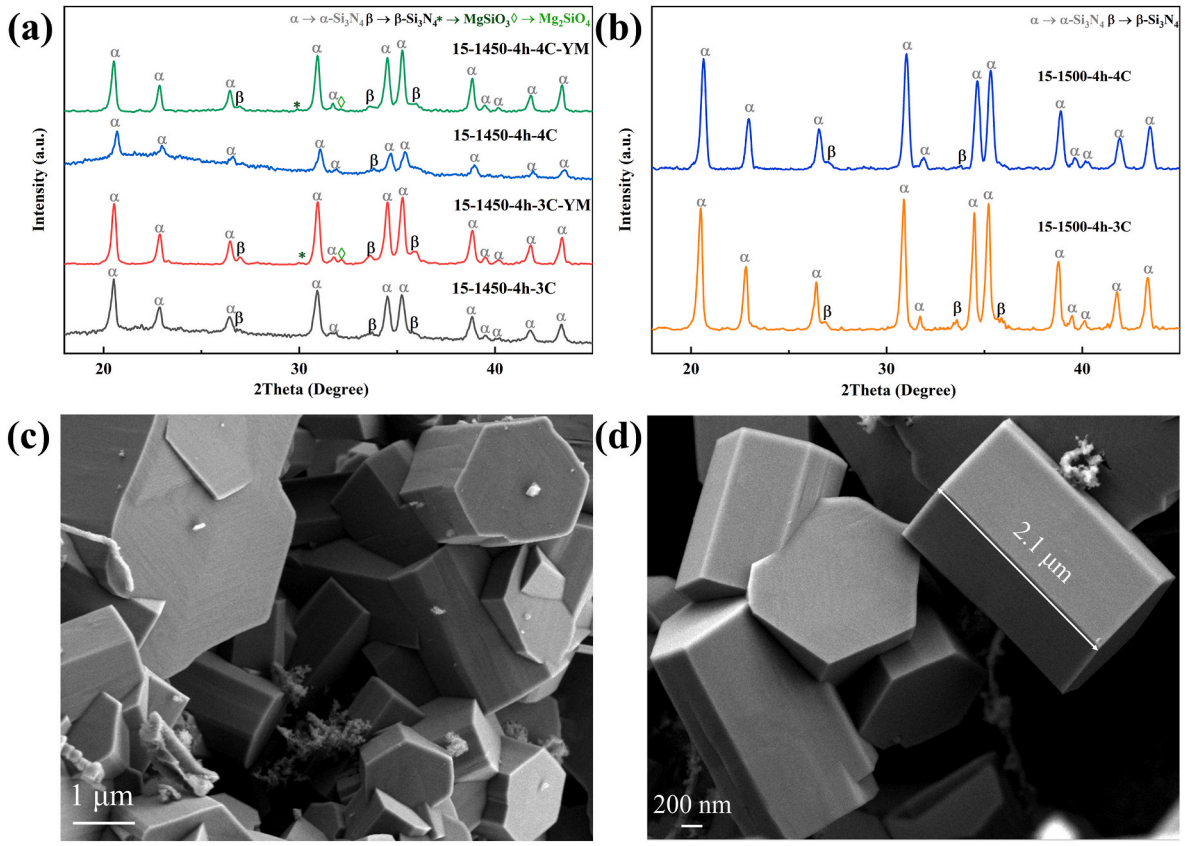

Fig. 12. **(A)** XRD patterns of Si_3N_4 powder synthesized with or without added sintering aids; **(b)** XRD patterns of Si_3N_4 powder synthesized at 1500 °C for 4 h without added sintering aids; **(c)** and **(d)** SEM images of the high purity α-Si_3N_4 labeled 15-1500-4h-4C.

100 and the C/Si ratio of 3. The morphology of the β-Si_3N_4 mainly consisted of rod-like whiskers with a length of approximately 1.4 μm.

(2) By utilizing $YCl_3{\cdot}6H_2O$ and $MgCl_2$ as sintering aids along with the H_2O/TEOS ratio of 15 and the C/Si ratio of 4 at a reaction temperature of 1450 °C for 4 h, α-Si_3N_4 nano-powder with an α-phase content reaching up to 91 wt% could be synthesized. The powder exhibited uniform spherical particle with an average particle size around 70 nm.

(3) The water-soluble sintering aid $MgCl_2$ could form eutectic liquid phase with SiO_2 during the process. This could not only promote the phase transformation of α-Si_3N_4, but also reduce the synthesis temperature of CRN process. Without adding any sintering aids or Si_3N_4 seeds, high purity α-Si_3N_4 with an α content reaching 96 wt % could be prepared at 1500 °C for 4 h by using the H_2O/TEOS ratio of 15 and the C/Si ratio of 4. The morphology of α-Si_3N_4 exhibited extremely regular hexagonal prism shape, and grain length was approximately 2 μm.

CRediT authorship contribution statement

Yan Wang: Conceptualization, Writing – original draft. **Zeyu Wang:** Data curation. **Zeping Zhu:** Formal analysis. **Jiaqi Wang:** Supervision. **Ziyang Meng:** Data curation. **Deqiang Wang:** Conceptualization, Writing – review & editing.

Declaration of competing interest

The authors declare that they have no known competing financial interests or personal relationships that could have appeared to influence the work reported in this paper.

Acknowledgements

This research did not receive any specific grant from funding agencies in the public, commercial, or not-for-profit sectors.

Appendix A. Supplementary data

Supplementary data to this article can be found online at https://doi.org/10.1016/j.ceramint.2024.06.234.

References

[1] X. Hou, E. Wang, B. Li, J. Chen, K.C. Chou, Corrosion behavior of porous silicon nitride ceramics in different atmospheres, Ceram. Int. 43 (2017) 4344–4352, https://doi.org/10.1016/j.ceramint.2016.12.079.

[2] E. Wang, B. Li, Z. Yuan, J. Chen, K.C. Chou, X. Hou, Morphological evolution of porous silicon nitride ceramics at initial stage when exposed to water vapor, J. Alloys Compd. 725 (2017) 840–847, https://doi.org/10.1016/j.jallcom.2017.07.249.

[3] F. Hu, Z.P. Xie, J. Zhang, Z.L. Hu, D. An, Promising high-thermal-conductivity substrate material for high-power electronic device: silicon nitride ceramics, Rare Met. 39 (2020) 463–478, https://doi.org/10.1007/s12598-020-01376-7.

[4] D. Yao, H. Chen, K. hui Zuo, Y. Xia, J. Yin, H. Liang, Y.P. Zeng, High temperature mechanical properties of porous Si_3N_4 prepared via SRBSN, Ceram. Int. 44 (2018) 11966–11971, https://doi.org/10.1016/j.ceramint.2018.03.044.

[5] J.Q. Li, F. Luo, D.M. Zhu, W.C. Zhou, Influence of phase formation on dielectric properties of Si_3N_4 ceramics, J. Am. Ceram. Soc. 90 (2007) 1950–1952, https://doi.org/10.1111/j.1551-2916.2007.01716.x.

[6] S. Shahrestani, M.C. Ismail, S. Kakooei, M. Beheshti, Microstructure, phase compositions and mechanical properties of slip cast sintered SiC/Si_3N_4 composites, Ceram. Int. 47 (2021) 13173–13180, https://doi.org/10.1016/j.ceramint.2021.01.182.

[7] M. Zhou, D. Rodrigo, Y.B. Cheng, Effects of the electric current on conductive Si_3N_4/TiN composites in spark plasma sintering, J. Alloys Compd. 547 (2013) 51–58, https://doi.org/10.1016/j.jallcom.2012.08.091.

[8] C. Bagci, Q. Yang, W.M. Kriven, Formation of α/β-Si_3N_4 nanoparticles by carbothermal reduction and nitridation of geopolymers, J. Am. Ceram. Soc. 102 (2019) 6542–6551, https://doi.org/10.1111/jace.16545.

[9] M. Rezazadeh, R. Emadi, A. Saatchi, A. Ghasemi, The role of Y_2O_3 and MgO additives on the photoluminescence properties of Si_3N_4 nanoparticles, J. Cluster Sci. 27 (2016) 73–84, https://doi.org/10.1007/s10876-015-0909-3.
[10] B. Li, Y. Feng, G. Li, H. Chen, J. Chen, X. Hou, Preparation of high-purity α-Si_3N_4 nano-powder by precursor-carbothermal reduction and nitridation, Ceram. Int. 45 (2019) 6335–6339, https://doi.org/10.1016/j.ceramint.2018.12.118.
[11] K. Sardar, R. Bounds, M. Carravetta, G. Cutts, J.S.J. Hargreaves, A.L. Hector, J. A. Hriljac, W. Levason, F. Wilson, Sol-gel preparation of low oxygen content, high surface area silicon nitride and imidonitride materials, Dalton Trans. 45 (2016) 5765–5774, https://doi.org/10.1039/c5dt04961j.
[12] L. Wang, G. He, X. Wu, Q. Meng, S. Deng, Z. Yang, J. Li, Effect of Si particle size and NH_4Cl additive on combustion synthesis of α-Si_3N_4, Ceram. Int. 45 (2019) 21635–21639, https://doi.org/10.1016/j.ceramint.2019.07.160.
[13] K. Raju, S. Moon, M. Kim, H.N. Kim, H.K. Lee, J. Cho, Cost-effective preparation of high-quality silicon nitride powders from silicon scrap through direct nitridation, Ceram. Int. 49 (2023) 34872–34879, https://doi.org/10.1016/j.ceramint.2023.08.161.
[14] A. Qadir, P. Pinke, J. Dusza, Silicon nitride-based composites with the addition of cnts—a review of recent progress, challenges, and future prospects. https://doi.org/10.3390/ma13122799, 2020.
[15] Z. Wang, L. Wang, Q. Qi, Q. Wu, N. Cui, T. Li, Y. Yu, H. Tang, Z. Qiao, Influence of alumina on the formation process and morphology of silicon nitride whisker, J. Cryst. Growth 619 (2023) 127338, https://doi.org/10.1016/j.jcrysgro.2023.127338.
[16] B. Li, G. Li, J. Chen, H. Chen, X. Xing, X. Hou, Y. Li, Formation mechanism of elongated β–Si_3N_4 crystals in Fe–Si_3N_4 composite via flash combustion, Ceram. Int. 44 (2018) 9395–9400, https://doi.org/10.1016/j.ceramint.2018.02.155.
[17] A. Shimamura, Y. Hotta, H. Hyuga, M. Hotta, K. Hirao, Improving the thermal conductivity of epoxy composites using a combustion-synthesized aggregated β-Si_3N_4 filler with randomly oriented grains, Sci. Rep. 10 (2020) 1–9, https://doi.org/10.1038/s41598-020-71745-w.
[18] H. Ji, Z. Huang, K. Chen, W. Li, Y. Gao, M. Fang, Y. gai Liu, X. Wu, Synthesis of Si_3N_4 powder with tunable α/β-Si_3N_4 content from waste silica fume using carbothermal reduction nitridation, Powder Technol. 252 (2014) 51–55, https://doi.org/10.1016/j.powtec.2013.10.030.
[19] H. Xing, B. Liu, J. Sun, B. Zou, Mechanical properties of Si_3N_4 ceramics from an in-situ synthesized a-Si_3N_4/β-Si_3N_4 composite powder, Ceram. Int. 43 (2017) 2150–2154, https://doi.org/10.1016/j.ceramint.2016.10.196.
[20] C.L. Yeh, F.S. Wu, Y.L. Chen, Effects of α- and β-Si_3N_4 as precursors on combustion synthesis of (α+β)-SiAlON composites, J. Alloys Compd. 509 (2011) 3985–3990, https://doi.org/10.1016/j.jallcom.2010.12.201.
[21] S.Y. Sun, Y.Y. Ge, Q. Wang, Z.B. Tian, J. Zhang, W. Cui, G. hua Liu, K.X. Chen, Synthesis and growth mechanism of single crystal β-Si_3N_4 particles with a quasi-spherical morphology, J. Am. Ceram. Soc. 101 (2018) 4526–4537, https://doi.org/10.1111/jace.15710.
[22] S.Y. Sun, Q. Wang, Y.Y. Ge, Z.B. Tian, J. Zhang, Z. peng Xie, Synthesis of well-dispersed columnar Si_3N_4 using carbothermal reduction–nitridation method, Powder Technol. 331 (2018) 322–325, https://doi.org/10.1016/j.powtec.2018.03.046.
[23] S.Y. Sun, Z.B. Tian, J. Zhang, K.X. Chen, Z. peng Xie, Carbothermal synthesis of micron-sized β-Si_3N_4 with tailored morphology, Ceram. Int. 43 (2017) 17243–17246, https://doi.org/10.1016/j.ceramint.2017.09.114.
[24] N. Karakuş, A.O. Kurt, H.Ö. Toplan, Synthesizing high α-phase Si_3N_4 powders containing sintering additives, Ceram. Int. 35 (2009) 2381–2385, https://doi.org/10.1016/j.ceramint.2009.02.002.
[25] T.M. Karnaukhov, A.A. Vedyagin, S.V. Cherepanova, V.A. Rogov, I.V. Mishakov, Sol–gel synthesis and characterization of the binary Ni–Mg–O oxide system, J. Sol. Gel Sci. Technol. 92 (2019) 208–214, https://doi.org/10.1007/s10971-019-05076-2.
[26] G.Q. Tan, H.Y. Miao, H.J. Ren, Z.W. Yu, J. Li, H.Q. Li, Synthesizing silicon nitride whiskers by solvothermal and carbothermal methods, Key Eng. Mater. 368–372 (2008) 868–870. https://doi.org/10.4028/www.scientific.net/kem.368-372.868.
[27] Z. Omidi, A. Ghasemi, S.R. Bakhshi, Synthesis and characterization of Si_3N_4 wires from binary carbonaceous silica aerogels, Powder Technol. 252 (2014) 20–24, https://doi.org/10.1016/j.powtec.2013.10.024.
[28] C. Ma, Y. Li, P. Jiang, X. Yue, Synthesis mechanism of α-Si_3N_4 whiskers via SiO vapor in reaction bonded Si_3N_4-SiC composite, J. Alloys Compd. 938 (2023) 168723, https://doi.org/10.1016/j.jallcom.2023.168723.
[29] Y. Wang, H. Wu, B. Jia, D. Zhang, Y. Zhang, Z. Zhang, C. Liu, J. Tian, M. Qin, X. Qu, Synthesis of monodisperse and high-purity α-Si_3N_4 powder by carbothermal reduction and nitridation, Adv. Powder Technol. 32 (2021) 3101–3106, https://doi.org/10.1016/j.apt.2021.06.023.
[30] K. Chen, Z. Huang, Y.G. Liu, M. Fang, J. Huang, Y. Xu, Synthesis of β-Si_3N_4 powder from quartz via carbothermal reduction nitridation, Powder Technol. 235 (2013) 728–734, https://doi.org/10.1016/j.powtec.2012.11.036.
[31] Y. Wang, J. Tian, H. Wu, B. Jia, X. Li, Y. Zhang, Z. Zhang, X. Qu, M. Qin, Thermal and mechanical properties of Si_3N_4 ceramics obtained via two-step sintering, Ceram. Int. 48 (2022) 18294–18301, https://doi.org/10.1016/j.ceramint.2022.03.088.
[32] A. Atasoy, The growth and the reaction mechanism of Si_3N_4 powder from silica, Mater. Sci. Forum 554 (2007) 157–162. https://doi.org/10.4028/www.scientific.net/msf.554.157.
[33] S.J.P. Durham, K. Shanker, R.A.L. Drew, Carbothermal synthesis of silicon nitride: effect of reaction conditions, J. Am. Ceram. Soc. 74 (1991) 31–37, https://doi.org/10.1111/j.1151-2916.1991.tb07292.x.
[34] A. Venkateswara Rao, S.D. Bhagat, Synthesis and physical properties of TEOS-based silica aerogels prepared by two step (acid-base) sol-gel process, Solid State Sci. 6 (2004) 945–952, https://doi.org/10.1016/j.solidstatesciences.2004.04.010.
[35] D.A. Gould, M. Quinlan, M.P. Albano, L.B. Garrido, L.A. Genova, K.P. Plucknett, A simple method for synthesis of acicular β-Si_3N_4 seed crystals, Ceram. Int. 35 (2009) 1357–1362, https://doi.org/10.1016/j.ceramint.2008.07.013.
[36] Z. Hu, J. Liu, Z. Xie, Synthesis of α-Si_3N_4 whiskers or equiaxed particles from amorphous Si_3N_4 powders, Ceram. Int. 46 (2020) 23734–23741, https://doi.org/10.1016/j.ceramint.2020.06.147.
[37] B. Li, J. hong Chen, J. dong Su, M. wei Yan, J. lin Sun, Y. Li, Morphology of α-Si_3N_4 in Fe–Si3N4 prepared via flash combustion, Int. J. Miner. Metall. Mater. 22 (2015) 1322–1327, https://doi.org/10.1007/s12613-015-1200-1.
[38] F. Wang, X. Qin, G. Jin, X. Guo, Temperature-controlled synthesis of Si_3N_4 nanomaterials via direct nitridation of Si powders, Phys. E Low-Dimensional Syst. Nanostructures. 42 (2010) 2033–2035, https://doi.org/10.1016/j.physe.2010.03.017.
[39] M.D. Alcalá, J.M. Criado, C. Real, Influence of the experimental conditions and the grinding of the starting materials on the structure of silicon nitride synthesised by carbothermal reduction, Solid State Ionics 141–142 (2001) 657–661, https://doi.org/10.1016/S0167-2738(01)00800-1.
[40] A.W. Weimer, G.A. Eisman, D.W. Susnitzky, D.R. Beaman, J.W. McCoy, Mechanism and kinetics of the carbothermal nitridation synthesis of α-silicon nitride, J. Am. Ceram. Soc. 80 (1997) 2853–2863, https://doi.org/10.1111/j.1151-2916.1997.tb03203.x.
[41] X.J. Liu, Z.Y. Huang, Q.M. Ge, X.W. Sun, L.P. Huang, Microstructure and mechanical properties of silicon nitride ceramics prepared by pressureless sintering with MgO-Al_2O_3-SiO_2 as sintering additive, J. Eur. Ceram. Soc. 25 (2005) 3353–3359, https://doi.org/10.1016/j.jeurceramsoc.2004.08.025.